THE JOURNAL OF PHYSICAL CHEMISTRY A

Article

Cite This: J. Phys. Chem. A 2019, 123, 9612−9620

pubs.acs.org/JPCA

Combined High-Resolution Optical Tweezers and Multicolor Single-Molecule Fluorescence with an Automated Single-Molecule Assembly Line

Cho-Ying Chuang, Matthew Zammit, Miles L. Whitmore, and Matthew J. Comstock*

Department of Physics and Astronomy, Michigan State University, East Lansing, Michigan 48824, United States

Supporting Information

ABSTRACT: We present an instrument that combines high-resolution optical tweezers and multicolor confocal fluorescence spectroscopy along with automated single-molecule assembly. The multicolor allows the simultaneous observation of multiple molecules or multiple degrees of freedom, which allows, for example, the observation of multiple proteins simultaneously within a complex. The instrument incorporates three fluorescence excitation lasers, with a reliable alignment scheme, which will allow three independent fluorescent probe or FRET measurements and also increases flexibility in the choice of fluorescent molecules. We demonstrate the ability to simultaneously measure angstrom-scale changes in tether extension and fluorescence signals. Simultaneous tweezers and fluorescence measurement are particularly challenging because of fluorophore photobleaching, even more so if multiple fluorophores are to be measured. Therefore, (1) fluorescence excitation and detection is interlaced with time-shared dual optical traps. (2) We investigated the photostability of common fluorophores. The mean number of photons emitted before bleaching was unaffected by the trap laser and decreased only slightly with increasing excitation laser intensity. Surprisingly, we found that Cy5 outperforms other commonly used fluorophores by more than fivefold. (3) We devised computer-controlled automation, which conserves fluorophore lifetime by quickly detecting fluorophore-labeled molecule binding, turning off lasers, and moving to add the next fluorophore-labeled component. The single-molecule assembly line enables the precise assembly of multimolecule complexes while preserving fluorophores.

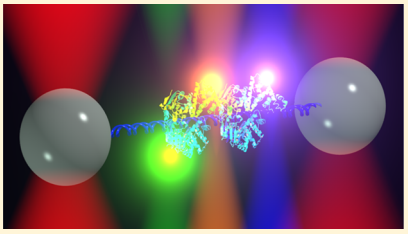

INTRODUCTION

Over the last 2 decades, single-molecule measurement methods have become powerful tools to investigate fundamental biological molecular activity by directly observing individual molecules in action. Details of step-wise reaction kinetics can be observed, which otherwise would be averaged out in traditional ensemble measurements. Two major single-molecule methods are force- and fluorescence-based measurements. Force-based measurements, as via optical tweezers, magnetic tweezers, or atomic force microscopes, can be used to observe the motions and conformations of individual proteins for long time durations over large distances with sub-nanometer resolution.[1−3] In addition, applied force can tune molecular stability and probe reaction free energy landscapes. Single-molecule fluorescence methods can also be used to detect the motion and conformation of individual molecules,[4,5] though often with reduced resolution and shorter observation times (because of photobleaching). However, biological protein machinery generally possesses multiple reaction degrees of freedom and assembles into complexes composed of many interacting molecules. Any individual single-molecule method is generally limited in its capability to directly observe such complexity. Recent progress has been made by devising instruments and methods that combine force and fluorescence measurements, allowing the simultaneous observation of complex multiprotein or multi-degree of freedom systems.[6−15] A hybrid instrument that combined high-resolution optical tweezers with a single-color confocal microscope showed the promise of the method by directly revealing how helicase conformation and oligomeric state couple to DNA unwinding activity.[9,16] To make further progress, we need to increase the number of fluorescence excitation and detection channels integrated into the instrument. Whereas multicolor confocal fluorescence microscopes have existed for some time, it is not trivial to integrate these into a high-resolution optical tweezers instrument in part because: (1) high powered optical trapping lasers tend to quickly photobleach fluorophores before measurements can take place, (2) high-resolution tweezers are complicated instruments that must be modified carefully in order to preserve their performance, and (3) increasing the number of fluorophores increases the likelihood that at least one of them will bleach and prematurely end the measurement. Especially, high efficiency data acquisition is crucial as high-resolution force measurements cannot be made in parallel.

Here, we present a multicolor hybrid instrument that combines three fluorescence excitation and detection channels with dual-trap high-resolution optical tweezers along with enhanced computer automation (Figure 1a). We developed a set of protocols to simply and precisely align the confocal spot with the tweezers with ultimate verification by directly imaging

Received: August 30, 2019
Revised: October 16, 2019
Published: October 17, 2019

DOI: 10.1021/acs.jpca.9b08282
J. Phys. Chem. A 2019, 123, 9612−9620

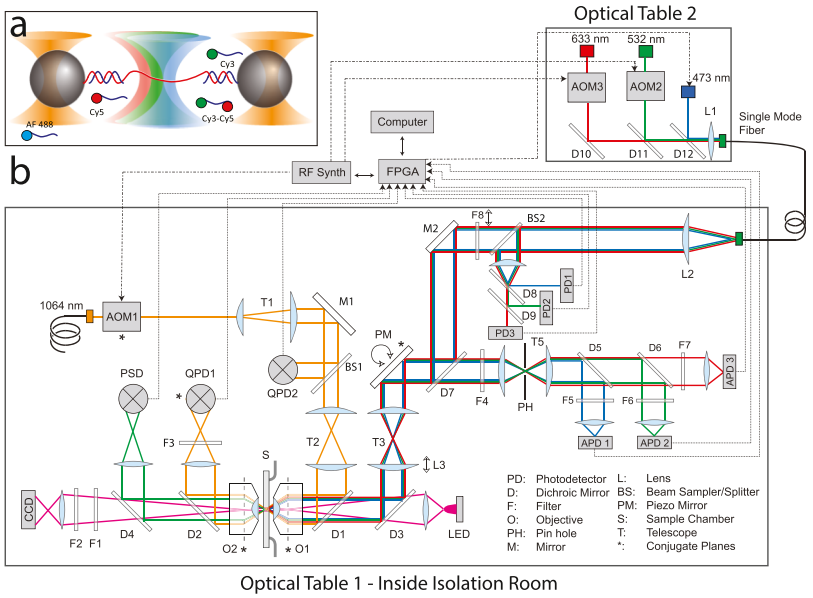

Figure 1. Instrument concept and schematic. (a) Cartoon of multicolor fleezers instrument concept: high-resolution dual-trap optical tweezers (laser traps represented by orange cones) trapping a pair of beads (gray spheres) tethered together by a single DNA molecule to which a variety of fluorophore-labeled ssDNA probe molecules can bind and be excited and detected using a trio of confocal excitation lasers (represented by the blue, green, and red cones centered on the DNA tether molecule). (b) Instrument layout showing essential components and optical paths. The multicolor optical tweezers instrument contains three modules: optical tweezers (orange solid lines), three-color confocal fluorescence excitation and emission (green, red, and blue solid lines), and bright-field imaging system (magenta solid lines). The majority of the instrument is assembled on optical Table 1 located inside a sound-proof, temperature-controlled isolation room. The fluorescence excitation laser sources are located on a second optical table outside this room and are all coupled to a single optical fiber for transport to the main instrument table. The dashed lines indicate the back-focal planes of the objectives and the asterisks indicate planes conjugate to it. Arrows indicate adjustable translation or rotation stages. A full description is in the text and a detailed parts list is provided in the Supporting Information Note.

a bright inorganic quantum dot bound to a tether at a force-dependent "cryptic binding site". We demonstrated the high-resolution tweezers and fluorescence performance by measuring sub-nanometer tether extension changes and accompanying single fluorophore signals upon the annealing and melting of fluorophore-labeled short ssDNA probes to a tethered strand of DNA. We evaluated the performance of the most commonly used organic fluorophores and surprisingly found that Cy5 and related fluorophores outperformed Cy3. To minimize photobleaching and improve data acquisition efficiency, we devised a precise computer-controlled single-molecule assembly line. The sample chamber contains multiple adjacent laminar flow fluid streams containing different labeled molecules, which bind to specific sites on a DNA tether. The computer automatically moves the trapped tether molecule between fluid streams, turning on the corresponding excitation laser only until a molecule is detected binding, and then moving on to the next stream. This process minimally wastes fluorescence and maximizes fluorophore lifetime. All instrument control software is made available. We believe these methods will be broadly applicable to many research groups involved in a wide range of single molecule protein−nucleic acid investigations.

MATERIAL AND METHODS

DNA Tether Construct Preparation. Three types of DNA construct were used: (1) "probe cryptic hairpin binding", (2) "probe hybridization", and (3) "ligated probe". The probe cryptic hairpin binding construct was used for confocal alignment, the probe hybridization construct was used for dynamic DNA probe binding and unbinding experiments, and the ligated probe construct was used for fluorophore bleaching lifetime measurements. These constructs were similarly designed in a modular fashion with the sticky end ligation of two approximately 1.5 kb long double-stranded DNA (dsDNA) handles with the 5′ and 3′ complementary ends of a construct-specific DNA insert. Handle precursors were produced by polymerase chain reaction (PCR) with the left and right handles (LH and RH) functionalized with biotin and digoxigenin, respectively, via labeled primers for eventual attachment to anti-digoxigenin- and streptavidin-coated beads. The PCR products were then digested by restriction enzymes to expose single-stranded DNA (ssDNA) overhangs (sticky ends). The 5′ and 3′ end sequences of the inserts were complementary to the LH and RH overhands respectively. The handles and inserts were annealed and ligated together by T4 ligase using the standard protocol (New England Biolabs [NEB]). The desired final constructs were purified via a 1% agarose gel and cleaned up via a standard nucleic acid gel extraction kit (Qiagen).

The probe cryptic binding hairpin construct consisted of two 1.5 kb dsDNA handles (LH and RH) annealed and ligated to an 89-bp dsDNA hairpin plus tetra-loop with 5′ and 3′ ends complementary to the LH and RH sticky ends. The final construct contained a central hairpin with a sequence matching a complementary ssDNA oligomer probe molecule. This probe-binding site is only accessible when the tweezers pulls open a tethered hairpin.

The probe hybridization construct consisted of a 1.5 kb dsDNA handle (LH) and a 1.7 kb dsDNA handle (RH) annealed and ligated to a variable length ssDNA insert with 5′ and 3′ ends complementary to the LH and RH sticky ends. The ssDNA insert contained either one or two probe-binding

DOI: 10.1021/acs.jpca.9b08282
J. Phys. Chem. A 2019, 123, 9612−9620

sequences separated from the handles and/or each other by 5-dT spacer sequences.

The ligated probe construct was similar to the probe hybridization construct, except that the 5-dT handle spacer sequence on the 3′ end was removed, so that a 5′-phosphorylated and 3′-fluorophore-labeled ssDNA oligomer probe could be annealed to the insert and ligated to the RH. The final construct has a single fluorophore permanently attached in the center.

The sequences of the probe strands and inserts are shown in the Supporting Information Tables S1−S3.

Experiment Conditions. Measurements were conducted at 23 °C in a laminar fluid flow sample chamber (e.g., Figure 5a).[17] The custom-made sample chambers consisted of two no. 1 microscope cover glass (Fisher Scientific) sandwiching a sheet of parafilm with fluid channels precisely cut via a CO_2 laser engraver (Universal Laser Systems VLS2.30). Experiments were conducted in a central multichannel region. A pair of flanking channels containing either anti-digoxigenin− or DNA−streptavidin-coated beads were connected to the central channels by glass capillary tubes embedded in the parafilm. The multicolor assembly line experiments were conducted in chambers containing three central channels (Figure 5a) containing different labeled probe molecules. Flow was maintained in all fluid channels via computer-controlled syringe pumps (Harvard Apparatus) pushing on gas-tight glass syringes (Hamilton) to ensure smooth flowing buffer streams that do not mix. The DNA tether constructs were first incubated with streptavidin-coated polystyrene beads (800 nm diameter, Spherotech) for 30 min at room temperature, then diluted into sample buffer before single-molecule experiments. A single construct molecule was tethered in situ between a trapped DNA−streptavidin-coated bead and a trapped anti-digoxigenin-coated bead (800 nm diameter, Spherotech).

For the cryptic binding alignment experiments, the sample buffer contained 100 mM Tris-HCl pH 8, 50 mM NaCl, 20 mM $MgCl_2$, 2 mM trolox, 7.5 nM Qdot705-labeled probes (Qdot 705 streptavidin conjugate, Q10163MP, Invitrogen), and an oxygen scavenging system. For the fluorophore bleaching lifetime experiments, the sample buffer contained 100 mM Tris-HCl, pH 8, 50 mM NaCl, 2 mM trolox, and an oxygen scavenging system. For the DNA probe-binding experiments, the sample buffer was chosen to optimize the probe-binding and -unbinding rates and contained 20 mM Tris-HCl, pH 8, 100 mM NaCl, 20 mM $MgCl_2$, 2 mM trolox, 5−10 nM fluorophore-labeled probes, and an oxygen scavenging system. The oxygen scavenging system consisting of 1% glucose and 1% either pyranose oxidase or glucose oxidase together with catalase was used to improve fluorophore and tether lifetimes.[18,19] Trolox is a triplet-state quencher that reduces blinking and photobleaching.[20]

Data Analysis and Modeling. Data analysis was performed using standard methods implemented via custom codes programmed in MATLAB version 2016b (MathWorks). Data were recorded at 66.7 kHz and then boxcar-averaged to a final lower rate (20 ms per data point) for analysis and plotting. Fluorophore-labeled probe-binding, -unbinding or photobleaching events were found by an automated routine identifying local maxima and minima above the noise threshold in the derivative of the data. Steps were verified by the eye. Tether extension changes were evaluated at these same fluorescence step locations (e.g., Figure 3b). The distributions of fluorophore bleaching times and photon counts before bleaching were all well-described by single exponential models. Thus, the fluorophore photobleaching lifetime and expected total photon number were determined from the mean of the set of individual fluorophore bleaching times and photon counts, which is the maximum likelihood estimator. Error bars are the standard error of the mean.

Standard polymer models of DNA[21,22] were used to calculate the extension of DNA. The extension of dsDNA handles was computed by an extensible worm-like chain model, and the extension of ssDNA insert was computed by an extensible freely jointed chain model. For dsDNA, the persistence length was 53 nm, the contour length per base pair was 0.34 nm, and the stretch modulus was 1200 pN. For ssDNA, the persistence length was 0.75 nm, the contour length per nucleotide was 0.59 nm, and the stretch modulus was 800 pN.

RESULTS AND DISCUSSION

We previously showed that high-resolution optical tweezers measurements and single-molecule fluorescence measurements could be combined successfully by interlacing confocal fluorescence excitation and detection with time-shared dual-

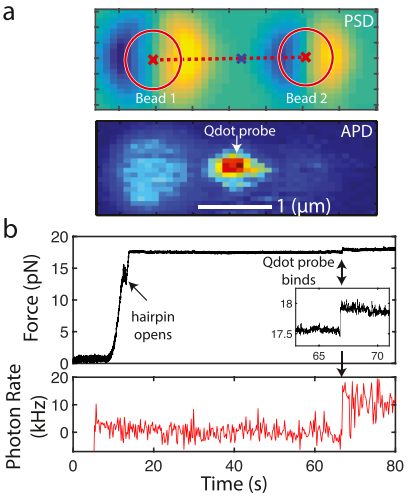

Figure 2. Alignment of confocal fluorescence module with tweezers. (a) Confocal excitation laser raster scan (green laser) across the region of two trapped and tethered beads. Upper: bead position detection x signal from PSD with the false color yellow and blue indicating a more positive and negative x signal, respectively. Beads are seen on the left and right with the "x" symbols, indicating the best fit bead centers, the red circles the approximate bead surfaces (800 nm diameter), the red dashed line the approximate tether alignment, and the blue "x" symbol the best calculated location of the fluorophore-labeled probe-binding site. Below is raster scan of the same area with the excitation laser power reduced to the usual single-fluorophore level (10 000× dimmer) and measurement made by the APD 1 green channel single photon detector. The beads are dimly visible. A single quantum dot-labeled probe molecule is visibly bound to the tether between the beads at the predicted location. (b) A hairpin tether construct contains a "cryptic binding site" within the hairpin that is only accessible upon unzipping of the hairpin under force. Upper: the hairpin is pulled to a high force and opens at ∼15 pN. Subsequently, a quantum dot-labeled DNA oligonucleotide probe molecule binds to the unzipped hairpin as seen by the sudden stepwise increase in force (zoom-in in lower right corner) and the simultaneous stepwise increase in fluorescence. The long-lived quantum dot is imaged in (a). The dimness of the bead images indicates no probes have bound to the beads.

DOI: 10.1021/acs.jpca.9b08282
J. Phys. Chem. A 2019, 123, 9612−9620

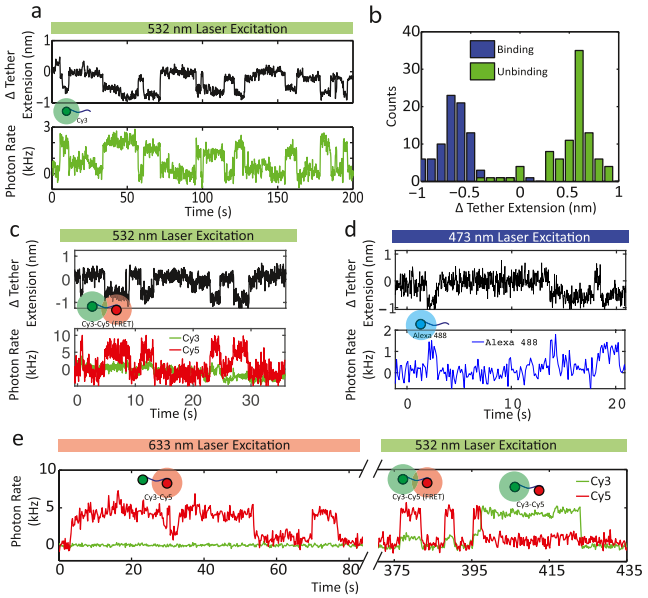

Figure 3. Multicolor fluorophore-labeled oligonucleotide hybridization experiment. A variety of measurements showing simultaneous high-resolution tweezers and fluorescence measurements for three colors and FRET. Tether tension is 10 pN for all and data were boxcar averaged to 30 ms per point. (a) Simultaneous measurement of tether extension (upper) and fluorescence (lower, green laser excitation, and detection channel APD 1) upon Cy3 fluorophore labeled probe binding and unbinding. The binding (and unbinding) events are indicated by the simultaneous stepwise decrease (and increase) in tether extension and increase (and decrease) of fluorescence. (b) Distribution of measured change in extension for many binding and unbinding events for the molecule in (a). (c) Similar to (a) but probe molecules include Cy5 fluorophores in addition and excitation by the green laser generates a FRET signal instead, as seen in the stepwise increases and decreases in the red detection channel (APD 2). (d) Similar to (a) but probe molecules are labeled with Alexa Fluor 488 and excited by the blue laser. For this shorter-lived fluorophore, photobleaching prior to probe unbinding is also observed, as at t = 15 s. (e) Cy3−Cy5 dual-labeled probes were excited by red and then green lasers in sequence. For t = 0−80 s, the Cy5 acceptor from the FRET probes were directly excited by the red laser and detected. For t = 370−435 s, the Cy3 donor was excited by the green laser producing FRET. At t = 400 s, an example of Cy5 photobleaching is seen.

trap optical tweezers.[9,23,24] Dual-trap optical tweezers achieve high resolution in part by suspending a DNA tether between a pair of beads trapped by a pair of traps created from a single laser, thus minimizing measurement drift and noise.[25] Confocal fluorescence excitation and detection optimally detects single photon fluorescence at the single tether location. In the combined instrument, photobleaching is avoided by turning the optical trap and fluorescence excitation lasers on and off asynchronously so that excited fluorophores are never exposed to the bright and destructive trap laser. Acousto-optic devices were used to modulate the laser intensities as they can be controlled electronically at high speed and are nonmechanical devices that do not degrade the tweezers' performance by adding noise. Further, the tweezers acousto-optic device rapidly alternates the trap laser deflection, creating dual trap locations. To maintain trap quality, the laser switching rate is very high (overall 66 kHz rate, or 15 μs period). In order to precisely time many instrument control and data acquisition channels, a single field programmable gate array (FPGA)-based PC card (National Instruments PCIe-7852R) with 25 ns timing resolution was used as the master control for all instrument control and data acquisition. The custom instrument control software was programmed in LabVIEW version 2012 (National Instruments). The instrument was located in a sound-proof, temperature-controlled, dark room and controlled remotely outside the room to minimize measurement noise and drift.

We have now enabled multicolor fluorescence measurement capability, enabling independent excitation and detection of three different excitation and detection channels. Previously, it was a substantial challenge to precisely co-align a single fluorescence excitation and detection optical path with the location of the trapped tether molecule. Co-aligning additional freestanding lasers and optics would be prohibitively difficult. Instead, we now use a strategy of coupling all excitation lasers into one single-mode polarization maintaining optical fiber. This is done on a supplemental optical table located outside the isolation room in order to provide additional space and reduce the thermal and noise load on the room. The multicolor laser light that emerges from the single mode fiber can be co-aligned as if only a single laser as all three colors emerge as if optimally focused point sources at the fiber exit aperture and achromatic lenses are used throughout. The flexibility of the FPGA-based instrument control platform allowed us to expand the fluorescence channel control and measurement in a modular, parallel way.

The instrument consists of three modules: optical tweezers, three-color fluorescence confocal microscope, and bright-field imaging system. The schematic diagram of the instrument is illustrated in Figure 1b. A detailed parts list is provided in the Supporting Information. All LabVIEW instrument software and MATLAB data analysis code are freely available for download on our lab website (https://web.pa.msu.edu/people/comstock/software.html). Here, we focus on the design, construction, and demonstration of the multicolor fluorescence detection with high-resolution optical tweezers.

High-Resolution Optical Tweezers. Please note that detailed descriptions for optical tweezers instrument and alignment protocols are described extensively elsewhere.[23,24,26,27] Here, we provide a general overview and specific details pertaining to the multicolor high-resolution fleezers instrument.

The optical tweezers module begins with the trap laser, a 5 W single mode, polarization-maintaining 1064 nm fiber laser (IPG Photonics). We prefer the fiber laser design because of its cost-effectiveness and extremely high pointing stability. The trap laser passes through an optical isolator (to minimize back-reflected laser light-induced noise) and then a rotatable half-wave plate followed by a polarizing cube beam splitter and beam dump to allow trap power to be coarsely adjusted manually (not shown in Figure 1b). Generally, power is only dumped during trap alignment procedures for increased safety.

Next, the trap beam passes through the acousto-optic *modulator* AOM1, which splits the beam into a pair of traps by rapidly (67 kHz) alternating the trap laser deflection angle, resulting in two trap locations. We use the first-order diffracted beam (~50% of total trap power with careful alignment) and block all other orders. We note that whereas multiaxis, longer range (~20 μm) acousto-optic *deflectors* have been more commonly used in optical tweezers applications, the lower noise, single-axis AOM is better matched for limited range (<3 μm) high-resolution trapping applications. AOM1 is also used

DOI: 10.1021/acs.jpca.9b08282
J. Phys. Chem. A 2019, 123, 9612−9620

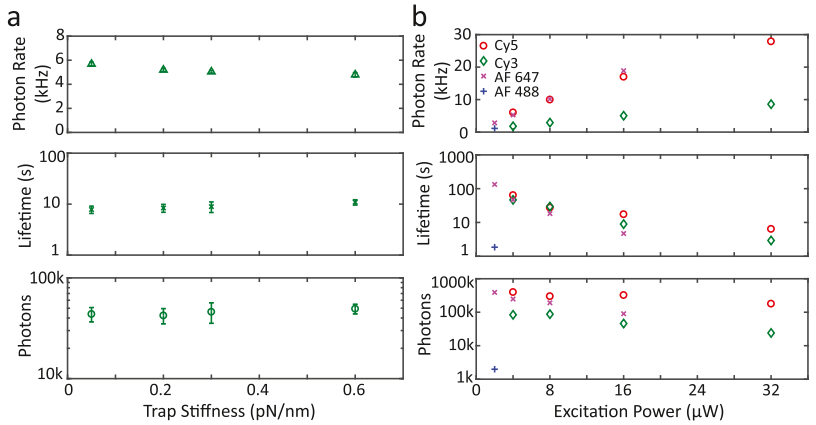

Figure 4. Fluorophore performance measurements. The ligated fluorophore probe construct was used to characterize fluorescence performance in the high-resolution fleezers instrument. (a) Effect of increasing trap laser intensity on fluorescence performance measuring tethered Cy3 fluorophores. 16 μW 532 nm excitation. Upper: fluorescence emission rate (kHz = 1000 photons/s), middle: mean fluorophore lifetime, lower: mean number of photons emitted, for trap stiffness 0.05, 0.2, 0.3, 0.6 pN/nm (error bars are standard error of the mean, with the number of molecules n = 29, 25, 28, and 27 respectively). (b) Effect of increasing fluorescence excitation laser on fluorophore performance for: Cy5 (red circle, excited by red laser, with n = 22, 28, 28, and 25 for 4, 8, 16, and 32 μW excitation, respectively), Cy3 (green diamond, excited by green laser, with n = 26, 14, 28, and 12 for 4, 8, 16, and 32 μW excitation, respectively), Alexa Fluor 647 (pink cross, excited by red laser, with n = 17, 23, 21, and 20 for 2, 4, 8, and 16 μW excitation, respectively), and Alexa Fluor 488 (blue plus, excited by blue laser at 2 μW, n = 30). Standard error of the mean error bars are smaller than symbol sizes. 0.3 pN/nm trap stiffness.

to interlace the traps with the fluorescence excitation lasers by turning the trap beam ON and OFF out-of-phase with the excitation lasers. That is, the sequence in time is: (1) trap 1 ON (trap 2 and fluorescence OFF, 5 μs), (2) trap 2 ON (trap 1 and fluorescence OFF, 5 μs), and (3) fluorescence excitation ON (traps 1 and 2 off, 5 μs) (Supporting Information Figure S1). The trap beams are completely off during the fluorescence interval as the RF signal that controls AOM1 is digitally generated and can be perfectly set to zero intensity. Important note: any unused trap laser power, including the full >5 W when both traps are off, emerges from AOM1 in the undiffracted zeroth order beam. This beam is carefully deflected via a small, highly reflective 1064 nm laser line mirror into a high-power beam dump. ~1% of the trap beam power is deflected by BS1 (a high quality, wedge-shaped beam splitter chosen to maintain the quality of the transmitted beam) to QPD2 to monitor each trap intensity. A proportional−integral−derivative (PID) feedback loop running on the FPGA monitors each trap intensity and adjusts the RF intensity into AOM1 for each trap in order to maintain constant trap power and thus trap stiffness at all times including when scanning the trap locations (e.g., during a force ramp measurement). Selection of the desired trap stiffness is made by choosing the appropriate trap beam intensity setpoint (as opposed to adjusting the half-wave plate of the beam splitting dump, as discussed above). Note that measurement of trap intensity and bead position must be carefully synchronized with interlacing timing. With the traps turning on and off, beads oscillate about their mean positions at the interlacing frequency (66 kHz, which is also the measurement frequency) with a typical amplitude of <10 nm, which is far less than the typical bead Brownian motion. In practice, any effects of the oscillating beads on measurement or the biological systems under study are undetectable.

Telescopes 1 and 2 expand the beam and transfer the image of the AOM1 deflection axis to the back aperture of the trap forming microscope objective O1 so that deflections of the trap laser do not clip the objective aperture. The objective is a high numerical aperture water immersion objective. A water immersion objective is chosen because unlike an oil objective, its focal properties are invariant with focal depth and thus trap and confocal properties remain unchanged, whereas the location within the sample chamber is changed. This is very important for being able to make consistent measurements in different sample fluid streams within the chamber.

The selection of the dichroic mirror (D1) that couples the trap laser beam with the visible fluorescence excitation, emission, and microscope illumination light is critical. All optics that the trap laser contacts need to be very high quality so as to not distort the beam and the subsequent traps. Typical 45° dichroic mirrors used in fluorescence applications are very thin so as to minimally achromatically shift images, whereas a thick mirror substrate is more typically desired to create an optically flat surface (e.g., 6.4 mm for the original high-resolution fluorescence tweezers instrument, both produced by CVI). We tested a selection of mirrors. Although the previous mirrors we used worked excellently for the trap beam, they did not perform well over the broad multicolor visible range. Our selected mirror (short-pass mirror with extended reflection and transmission on 3 mm thick fused silica, Chroma) performed perfectly over the full visible range and although slightly thinner did not show any trap beam distortion so long as the mirror was not mechanically clamped, but rather minimally epoxied to its mirror mount. The selection of the similar mirror D2 has less critical visible requirements as it does not impact on fluorescence measurements.

Trap laser light passing through the trapped beads was then collected by the back objective (O2) and sent to an IR-enhanced quadrant photodiode detector (QPD1) for measurement via the standard back-focal-plane interferometry technique. Bead positions and applied force within the trap were calibrated via the standard method of bead Brownian motion power spectra analysis.[28]

Bright-Field Imaging. The bright-field imaging system consists of a 940 nm infrared light-emitting diode as the illumination source and an IR-enhanced charge-coupled device (CCD) camera to image the sample chamber, beads, trap manipulation, tether formation, and so forth. F1 (short pass,

DOI: 10.1021/acs.jpca.9b08282
J. Phys. Chem. A 2019, 123, 9612−9620

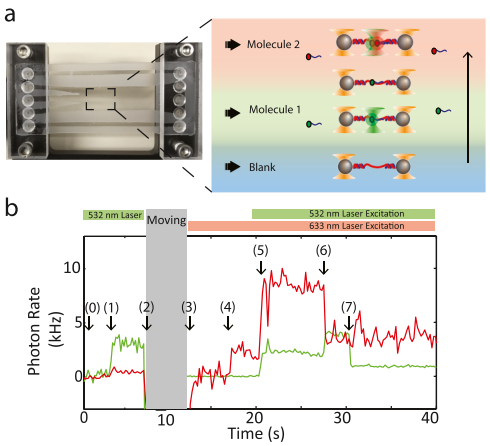

Figure 5. Molecular assembly line with multichannel flow chamber. Schematic of computer-automated assembly of fluorophore-labeled molecular complexes. (a) Left: photograph of a five-channel flow chamber assembled from cover glass sandwiching parafilm with laser cut channels. The top and bottom channels contain anti-digoxigenin and DNA-construct-coated streptavidin beads respectively connected to the central channels via capillary tubes. The central area consists of three adjacent laminar flow streams. Right: laminar flow stream layout. Lower: buffer without probe molecules ("blank"), middle: buffer containing Cy3-labeled probe molecules ("molecule 1"), and top: buffer containing Cy5-labeled probe molecules ("molecule 2"). The motorized sample stage moves the chamber vertically to transfer the trapped beads and tether between flow streams as indicated by the cartoons. Probe molecules in solution bind a site specifically to the tether and emit fluorescence when the computer turns on the appropriate excitation laser. (b) Example time trace for in situ molecular complex assembly. The automated sequence is as follows: the DNA tether was formed in "blank" buffer. (0) Transfer to the molecule 1 stream and green laser turned on. (1) A Cy3-labeled probe binds. (2) After a delay, the green laser is turned off and transfer to the molecule 2 stream is initiated. (3) Arrival at the molecule 2 stream and red laser turned on. (4) Cy5-labeled probe binds. (5) Green laser turned back on to verify that both probes are still bound and active as indicated by the FRET signal. (6) Cy5 fluorophores photobleach. (7) Cy3 fluorophore photobleaches.

1000 nm) and F2 (long-pass, 850 nm) were used to remove excess trap and fluorescence laser intensity as needed.

Multicolor Confocal Fluorescence Spectroscopy. Multicolor fluorescence measurements are enabled by three fluorescence excitation lasers, blue (473 nm), green (532 nm), and red (633 nm), that provide a wide spectral range and support the most common single molecule fluorophores including Alexa 488, Cy3, and Cy5 and their spectral equivalents. The lasers are interlaced with the dual traps, turning on only when the traps are off, for a 4 μs duration (Supporting Information Figure S1). For the green and red lasers, this is done by modulating AOM2 and AOM3 on and off, respectively. The blue laser is a diode laser with built-in high-speed electronic control that allows it to be directly modulated with a single digital signal from the FPGA. The three laser beams are coupled into a single single-mode polarization-maintaining optical fiber. Coupling is performed in free space for each collimated laser using a pair of mirrors (only one of which each is shown in Figure 1b), co-aligning to a high NA-molded aspheric lens, which is matched to the input aperture of the fiber. The lens and APC fiber input connector are held in high precision and stability rail-mounted holders and positioning stages (Qioptiq). High stability mounts and 1″ pedestals are used throughout to maximize long-term coupling stability (e.g., Newport Suprema mirror mounts). Approximately 50% laser coupling efficiency is easy to achieve and maintain and generally, there is a large excess of excitation power available for single fluorophore measurements.

The optical fiber is routed to the instrument table within the isolation room. The three beams emerge from the fiber output aperture as if from a single point source, differing only slightly in their divergence angles. They are jointly collimated by a single achromatic doublet lens. Subsequently, we use visible achromatic doublet lenses in the multicolor confocal path (e.g., for telescopes T3 and T5) to ensure consistent focusing and co-alignment of all lasers and fluorescence across the entire visible spectrum. A pellicle beam splitter (BS2) sends ∼5% of each laser to a set of silicon photodetectors (PD1, PD2, and PD3) for monitoring excitation laser intensity. Similar as for the trap, a set of three PID feedback loops running on the FPGA monitor each excitation laser intensity and adjust an analog output control signal to maintain constant laser intensity. For the red and green lasers, the FPGA analog out controls the respective AOM RF intensity and for the blue laser, the FPGA analog out directly controls the diode output. The piezo mirror stage (PM) provides lateral positioning of the excitation laser foci in the tether sample plane as well as raster scanning capability to produce images. Telescope T3 expands the lasers to their final collimated widths. We expand the lasers to approximately 1/2 the objective back aperture width to simplify co-alignment of the beams with the trap beams while maintaining near diffraction limited excitation laser foci volumes. The second lens of T3 is mounted on a translation stage, which is adjusted to adjust the focal plane of the lasers to match the optical traps. Dichroic mirror D3 reflects the excitation lasers into the front microscope objective (O1), which focuses the lasers to the tether sample plane. Fluorescence emitted from the excitation laser foci is collected by the same objective (O1) and then retrace the excitation laser optical paths in reverse until passing through the dichroic mirror D7, which reflects the excitation lasers in three narrow bands. A notch filter (F4) removes residual excitation laser intensity. Next, a lens focuses the fluorescence beam onto a pinhole confocal with the laser foci in the tether sample plane in order to suppress background fluorescence from out of the sample plane. The pinhole is mounted in a precision removable mount with ∼1 μm repeatability. For fluorescent lifetime measurements, the pinhole was removed to report the maximal signal. For all other measurements a 50 μm diameter pinhole was used, which reduced the single fluorophore signal by ∼50% while strongly suppressing background. However, we note that in many cases we find the pinhole is unnecessary and we remove it to maximize the signal. A subsequent lens recollimates the fluorescence beam, which is then split by a series of dichroic mirrors, filtered, and finally focused onto three avalanche photodiode (APD) single-photon detectors, one for each excitation and emission spectral band. To minimize background signal, APD photon counts are only accumulated during the fluorescence excitation laser ON periods. This is done by gating the FPGA photon counting digital inputs rather than using the APD hardware gate input as switching the APD hardware gate produces spurious false counts.

Precise alignment of the confocal excitation spot with the tethered molecule in the sample plane is essential in order to maximize fluorescence photon collection efficiency and signal to noise. We used multiple overlapping alignment methods,

DOI: 10.1021/acs.jpca.9b08282
J. Phys. Chem. A 2019, 123, 9612−9620

from coarse to fine positioning, to make the alignment process straightforward and reliable. Note that it is generally only necessary to observe one of the three excitation lasers during alignment protocols. We chose the green laser for convenience. First: the coarsest co-alignment of the excitation and trap lasers was achieved by simply observing the focused trap and excitation laser spots on the visible microscope CCD camera. The piezo mirror stage mount and mirror D3 were adjusted to overlap the spots laterally. The lens L3 was translated along the beam path to focus the excitation lasers in the same plane as the trap laser. Second: the excitation lasers can serve as back-focal-plane bead detection lasers (same principle as for trap laser bead detection). The piezo mirror raster-scans the excitation lasers across a pair of trapped beads, whereas a position-sensitive detector (PSD) records the x and y beam signals. Such a bead detection image for the x signal is shown in Figure 2b (the y signal also imaged from all three lasers showing co-alignment are shown in Supporting Information Figure S2). Fixing the piezo mirror position fixes the excitation laser location with respect to the beads and tether. The lens L3 was finely translated to adjust the excitation laser focal plane with respect to the beads. Coarsely, the excitation lasers are co-aligned with the trap plane when the detection images of the beads are minimum diameter (most in focus) and circular without distortion (Figure 2a). More precisely, we position the excitation laser lateral location at the center of one trapped bead in order to detect the motion of that bead and we then obtain the bead Brownian motion power spectra and calibration constants (the same method as for the trap laser bead detection method). The excitation lasers are co-aligned in the trap plane when the bead position measurement is maximally sensitive, or when the bead position calibration constant (i.e., volts to nm) is minimized. Further confirmation of the focal depth alignment can be made by trapping a 1 μm diameter fluorescent bead and measuring the fluorescence emitted with the confocal laterally aligned with the bead center while varying the focal depth (results from a typical alignment can be seen in the Supporting Information Figure S3). However, care must be taken with this method to not overexpose the bead during the process, which leads to photobleaching and possible misalignment. Once the focal depth alignment is finalized, it remains stable and does not require regular adjustment.

Precise lateral alignment of the confocal excitation location with the location of fluorescent probes on a tether is more demanding. The excitation lasers are more tightly focused laterally than axially (lateral width is approximately the excitation wavelength, i.e., ~500 nm width for the 532 nm excitation), making the lateral sensitivity greater. Trapped beads are often a source of background noise, particularly when fluorescent probes are attached to excess DNA on the DNA−streptavidin beads, and they are inevitably close to the excitation spot as tether lengths are kept short to maintain high-resolution tweezers measurement capability. To place the confocal spot laterally, we first find the centers of the beads using the PSD bead detection image. The bead centers are located at the intersection of the x signal image row and y signal image column that contain their respective image maxima. Using the known bead diameters, standard tether polymer modeling, and the known location of the fluorophore probe along the tether, we can then predict the lateral location of the fluorescent probe where we will locate the confocal spot (as in Figure 2a). To confirm the lateral location, we directly image a single fluorescent probe molecule attached to a tether. Although it is possible to directly image a single organic fluorophore (e.g., Cy3), it is extremely challenging because of the raster scan method confocal imaging inefficiency and photobleaching.[9] Inorganic fluorescent quantum dots are semiconductor particles with much brighter emission and reduced photobleaching.[29] These same properties mean they create a noisy background when either attached to probes in solution or directly attached to excess tether DNA on trapped beads. We devised a protocol to circumvent these issues by constructing tether molecules containing DNA hairpin inserts with sequences complementary to DNA oligomer probe molecules labeled with quantum dots. We use a dual-channel flow chamber containing adjacent channels with and without quantum-dot-oligomer probe molecules in solution. We form single tethers in the blank solution and then transfer to the quantum-dot-oligomer containing solution. We next increase the force on the tether to unzip the hairpin. A single quantum-dot-oligomer molecule will bind to the complementary exposed hairpin sequence (Figure 2b); they cannot bind to the excess DNA on the streptavidin bead because those DNA are not under tension and their hairpins remain zipped. We then return to the blank solution to image the tether (Figure 2a). In this way, we can image a single bright probe background-free and precisely confirm or correct our confocal lateral alignment. In general, likely drift of the piezo mirror stage requires us to acquire a bead detection scan image at the beginning of each trap session and use our quantum-dot-corrected tether model to place the confocal spot.

In order to demonstrate the new instrument capabilities, we measured the binding and unbinding of fluorophore-labeled 9 nucleotide-long single-stranded DNA oligonucleotides (DNA probes) to a strand of DNA tethered between a pair of trapped beads (Figure 3). The tethered DNA had a central section with an exposed ssDNA probe-binding site. Upon binding of a single probe molecule to the tethered DNA, the ssDNA section is converted to dsDNA, which results in a small (<1 nm) reduction in tether extension, which is detected by the high-resolution optical tweezers portion of the instrument. Simultaneously, the confocal fluorescence portion of the instrument detects the sudden presence of the fluorophore as a stepwise increase in fluorescence. Figure 3a shows an example simultaneous tether extension and fluorescence measurement for a Cy3 labeled probe excited by the green laser. A decrease/increase in tether extension is observed simultaneously with an increase/decrease in the fluorescence signal upon probe molecule binding/unbinding from the DNA tether. The distributions of the change in tether extension upon probe binding and unbinding for many reactions show clear sub-nanometer trap measurement resolution similar to the previous instrument (Figure 3b).[9] Example time traces demonstrate a variety of possible measurement configurations: Figure 3c: simultaneous trap and fluorescence measurement with the green laser exciting dual-labeled Cy3-Cy5 fluorescence resonance energy transfer (FRET) probes. Figure 3d: simultaneous trap and fluorescence measurement with the blue laser exciting Alexa Fluor 488 probes. Figure 3e: the red laser directly exciting the Cy5 acceptor of the dual-labeled Cy3−Cy5 FRET probes followed by green laser excitation.

We next quantitatively evaluated the performances of the most commonly used organic fluorophores for blue, green, and red excitation in our instrument. For this purpose, we constructed tethers with the fluorophore-labeled probe DNA

DOI: 10.1021/acs.jpca.9b08282
J. Phys. Chem. A 2019, 123, 9612−9620

already bound and permanently ligated to the tether. This way the loss of fluorescence signal unambiguously indicates photobleaching rather than the possible unbinding of the probe. We first investigated the effect of the trap on fluorescence performance using the most commonly used fluorophore, Cy3. The trap laser power was varied more than 10-fold over the typically used range corresponding to trap stiffness between 0.05 and 0.6 pN/nm, whereas the power of green excitation laser was kept constant at 16 μW. As seen in Figure 4a, the fluorophore emission intensity and lifetime were unchanged by varying the trap laser power, confirming that the interlacing method successfully protected the fluorophores from the trap laser.

Next, we measured the effect of the fluorescence excitation laser intensity on Alexa Fluor 488, Cy3, Cy5, and Alexa Fluor 647 fluorophores (Figure 4b). The fluorescence intensity is proportional to the excitation laser intensity as expected (Figure 4b upper panel). The photobleaching lifetime (Figure 4b middle panel) is inversely proportional to the excitation intensity, whereas the mean photon count before photobleaching (Figure 4b lower panel) was independent of excitation intensity, both as expected for these relatively low excitation intensities. Surprisingly, we found that the Cy5 performed much better than other fluorophores, particularly Cy3. Cy5 emits 5× more photons on average than Cy3 before photobleaching (400k vs 80k photons at low excitation power). Alexa Fluor 647 has an intensity similar to Cy5, but a slightly lower mean photon count. Alexa Fluor 488 has a substantially lower mean photon count prior to photobleaching (3k at low excitation power). Therefore, in order to optimize the performance in multicolor labeling experiments, fluorophore selection should be prioritized in the order of Cy5, then Cy3, and finally Alexa Fluor 488.

One common application of multicolor single molecule fluorescence methods is the direct observation of the stepwise assembly of individually labeled molecules into complexes. Adding high-resolution tweezers capability to multicolor fluorescence detection capability allows for new possibilities to observe the assembly of functioning complexes. However, when experiments depend on the observation of multiple fluorophores, the probability of any one fluorophore photobleaching multiplies and is a particular challenge for tweezers experiments, which must be conducted serially, one at a time. We have combined multichannel laminar flow sample chambers with precise computer control of fluorescence measurement and triggered chamber motion to implement an automated "molecular assembly line". This allows the precise addition of individual molecules of different types to a single DNA tether while conserving fluorescence photons and reducing photobleaching. Figure 5 shows an example of assembling a complex with two molecules in a chamber with three adjacent fluid channels. A single tether is formed and tested in the "blank" buffer which does not contain any fluorescent probe molecules. The motorized sample stage is then translated to the second channel containing Cy3-labeled probe molecule 1. The green laser is turned on automatically by the computer once the tether arrives at a set location (Figure 5b time label 0). The binding of a probe molecule (time label 1) is detected by the computer when the Cy3 channel signal (APD1) exceeds a pre-set background threshold. Next, the computer automatically turns the green laser off and initiates chamber motion to move the tether to the third channel containing Cy5-labeled probe molecule 2 (time label 2). Upon arrival, the computer turns on the red excitation laser (time label 3) and waits for the binding of a probe molecule by observing when the Cy5 channel signal (APD2) exceeds a pre-set background threshold (time label 4). A variety of measurements can subsequently be made. Here, we turn on the green laser again (time label 5) to verify that the first molecule we added, the Cy3-labeled probe molecule, is still present and active, as confirmed by the observed FRET signal (increase in APD2). Eventually, the Cy5 and then Cy3 fluorophores photobleach (time labels 6 and 7, respectively). Note that the delay time between the detection of the fluorophore-labeled molecule binding and the automatic turning off of the excitation laser and initiation of sample stage motion has been prolonged here to aid visualization. In practice, it can be reduced to <100 ms, depending on the brightness of the fluorophores and the background. Alternatively to fluorescence signal threshold detection, instead peaks in the derivative of the fluorescence signal can be detected. This can be advantageous when the background signal is variable (e.g., variable bead background noise), whereas the probe molecule fluorescence signal is generally constant. However, this method has a slightly delayed time response as it is necessary to integrate the signal a bit to reject noise. When appropriate, for example, for reversible reactions, the entire molecular assembly process can be automatically repeated indefinitely. In addition to the molecular assembly line protocol, our instrument software also includes many additional computer-automated protocols including similar dipping molecular assembly protocols integrated with force feedback measurements (e.g., as for helicase investigations[30]) and force-ramp and force-jump protocols (e.g., as for folding investigations[31]). Overall, we have found that automatic procedures such as this not only maximize measurement throughput by conserving fluorescent photons, but they dramatically reduce user error and fatigue.

■ ASSOCIATED CONTENT

Supporting Information

The Supporting Information is available free of charge on the ACS Publications website at DOI: 10.1021/acs.jpca.9b08282.

DNA oligomer sequences, instrument parts list, interlacing and time-sharing of optical traps and fluorescence lasers, PSD bead detection images, and alignment of confocal spot focal depth (PDF)

■ AUTHOR INFORMATION

Corresponding Author

*E-mail: mjcomsto@msu.edu. Phone: 517-884-5645.

ORCID

Matthew J. Comstock: 0000-0002-6931-285X

Author Contributions

The instrument was designed and built by C.-Y.C, M.L.W., and M.J.C. Testing and experiments were carried out by C.-Y.C, M.L.W., and M.Z. Data analysis was performed by C.-Y.C. C.-Y.C and M.J.C wrote the paper.

Notes

The authors declare no competing financial interest.

■ ACKNOWLEDGMENTS

This work was supported by a grant from the NSF (MCB-1919439) to M.J.C.

DOI: 10.1021/acs.jpca.9b08282
J. Phys. Chem. A 2019, 123, 9612−9620

REFERENCES

(1) Hinterdorfer, P.; Dufrêne, Y. F. Detection and Localization of Single Molecular Recognition Events Using Atomic Force Microscopy. *Nat. Methods* **2006**, *3*, 347−355.

(2) Moffitt, J. R.; Chemla, Y. R.; Smith, S. B.; Bustamante, C. Recent Advances in Optical Tweezers. *Annu. Rev. Biochem.* **2008**, *77*, 205−228.

(3) De Vlaminck, I.; Dekker, C. Recent Advances in Magnetic Tweezers. *Annu. Rev. Biophys.* **2012**, *41*, 453−472.

(4) Tinnefeld, P.; Sauer, M. Branching out of Single-Molecule Fluorescence Spectroscopy: Challenges for Chemistry and Influence on Biology. *Angew. Chem., Int. Ed.* **2005**, *44*, 2642−2671.

(5) Roy, R.; Hohng, S.; Ha, T. A Practical Guide to Single-Molecule FRET. *Nat. Methods* **2008**, *5*, 507−516.

(6) van Dijk, M. A.; Kapitein, L. C.; van Mameren, J.; Schmidt, C. F.; Peterman, E. J. G. Combining Optical Trapping and Single-Molecule Fluorescence Spectroscopy: Enhanced Photobleaching of Fluorophores. *J. Phys. Chem. B* **2004**, *108*, 6479−6484.

(7) Lang, M. J.; Fordyce, P. M.; Engh, A. M.; Neuman, K. C.; Block, S. M. Simultaneous, Coincident Optical Trapping and Single-Molecule Fluorescence. *Nat. Methods* **2004**, *1*, 133−139.

(8) Hohng, S.; Zhou, R.; Nahas, M. K.; Yu, J.; Schulten, K.; Lilley, D. M. J.; Ha, T. Fluorescence-Force Spectroscopy Maps Two-Dimensional Reaction Landscape of the Holliday Junction. *Science* **2007**, *318*, 279−283.

(9) Comstock, M. J.; Ha, T.; Chemla, Y. R. Ultrahigh-Resolution Optical Trap with Single-Fluorophore Sensitivity. *Nat. Methods* **2011**, *8*, 335−340.

(10) He, Y.; Lu, M.; Cao, J.; Lu, H. P. Manipulating Protein Conformations by Single-Molecule AFM-FRET Nanoscopy. *ACS Nano* **2012**, *6*, 1221−1229.

(11) Sirinakis, G.; Ren, Y.; Gao, Y.; Xi, Z.; Zhang, Y. Combined Versatile High-Resolution Optical Tweezers and Single-Molecule Fluorescence Microscopy. *Rev. Sci. Instrum.* **2012**, *83*, 093708.

(12) Forget, A. L.; Dombrowski, C. C.; Amitani, I.; Kowalczykowski, S. C. Exploring Protein-DNA Interactions in 3D Using in Situ Construction, Manipulation and Visualization of Individual DNA Dumbbells with Optical Traps, Microfluidics and Fluorescence Microscopy. *Nat. Protoc.* **2013**, *8*, 525−538.

(13) Heller, I.; Sitters, G.; Broekmans, O. D.; Farge, G.; Menges, C.; Wende, W.; Hell, S. W.; Peterman, E. J. G.; Wuite, G. J. L. Sted Nanoscopy Combined with Optical Tweezers Reveals Protein Dynamics on Densely Covered DNA. *Nat. Methods* **2013**, *10*, 910−916.

(14) Lee, S.; Hohng, S. An Optical Trap Combined with Three-Color FRET. *J. Am. Chem. Soc.* **2013**, *135*, 18260−18263.

(15) Kemmerich, F. E.; Swoboda, M.; Kauert, D. J.; Grieb, M. S.; Hahn, S.; Schwarz, F. W.; Seidel, R.; Schlierf, M. Simultaneous Single-Molecule Force and Fluorescence Sampling of DNA Nanostructure Conformations Using Magnetic Tweezers. *Nano Lett.* **2016**, *16*, 381−386.

(16) Comstock, M. J.; Whitley, K. D.; Jia, H.; Sokoloski, J.; Lohman, T. M.; Ha, T.; Chemla, Y. R. Direct observation of structure-function relationship in a nucleic acid-processing enzyme. *Science* **2015**, *348*, 352−354.

(17) Brewer, L. R.; Bianco, P. R. Laminar Flow Cells for Single-Molecule Studies of DNA-Protein Interactions. *Nat. Methods* **2008**, *5*, 517−525.

(18) Landry, M. P.; McCall, P. M.; Qi, Z.; Chemla, Y. R. Characterization of Photoactivated Singlet Oxygen Damage in Single-Molecule Optical Trap Experiments. *Biophys. J.* **2009**, *97*, 2128−2136.

(19) Swoboda, M.; Henig, J.; Cheng, H.-M.; Brugger, D.; Haltrich, D.; Plumeré, N.; Schlierf, M. Enzymatic Oxygen Scavenging for Photostability without pH Drop in Single-Molecule Experiments. *ACS Nano* **2012**, *6*, 6364−6369.

(20) Ha, T.; Tinnefeld, P. Photophysics of Fluorescent Probes for Single-Molecule Biophysics and Super-Resolution Imaging. *Annu. Rev. Phys. Chem.* **2012**, *63*, 595−617.

(21) Smith, S. B.; Cui, Y.; Bustamante, C.; Overstretching, B.-D. N. A. Overstretching B-DNA: The Elastic Response of Individual Double-Stranded and Single-Stranded DNA Molecules. *Science* **1996**, *271*, 795−799.

(22) Baumann, C. G.; Smith, S. B.; Bloomfield, V. A.; Bustamante, C. Ionic effects on the elasticity of single DNA molecules. *Proc. Natl. Acad. Sci. U.S.A.* **1997**, *94*, 6185−6190.

(23) Whitley, K. D.; Comstock, M. J.; Chemla, Y. R. High-Resolution "Fleezers": Dual-Trap Optical Tweezers Combined with Single-Molecule Fluorescence Detection. In *Optical Tweezers: Methods and Protocols*; Gennerich, A., Ed.; Springer New York: New York, NY, 2017; pp 183−256.

(24) Whitley, K. D.; Comstock, M. J.; Chemla, Y. R. High-Resolution Optical Tweezers Combined with Single-Molecule Confocal Microscopy. *Methods Enzymol.* **2017**, *582*, 137−169.

(25) Moffitt, J. R.; Chemla, Y. R.; Izhaky, D.; Bustamante, C. Differential Detection of Dual Traps Improves the Spatial Resolution of Optical Tweezers. *Proc. Natl. Acad. Sci. U.S.A.* **2006**, *103*, 9006−9011.

(26) Neuman, K. C.; Block, S. M. Optical Trapping. *Rev. Sci. Instrum.* **2004**, *75*, 2787−2809.

(27) van Mameren, J.; Wuite, G. J. L.; Heller, I. Introduction to Optical Tweezers: Background, System Designs, and Commercial Solutions. *Single Molecule Analysis*; Springer, 2011; Vol. *783*, pp 1−20.

(28) Berg-Sørensen, K.; Flyvbjerg, H. Power Spectrum Analysis for Optical Tweezers. *Rev. Sci. Instrum.* **2004**, *75*, 594−612.

(29) Alivisatos, A. P.; Gu, W.; Larabell, C. Quantum Dots as Cellular Probes. *Annu. Rev. Biomed. Eng.* **2005**, *7*, 55−76.

(30) Patrick, E. M.; Srinivasan, S.; Comstock, M. J. The RNA helicase Mtr4p is a duplex-sensing translocase. *Nat. Chem. Biol.* **2017**, *13*, 99−104.

(31) Izadi, D.; Chen, Y.; Whitmore, M. L.; Slivka, J. D.; Ching, K.; Lapidus, L. J.; Comstock, M. J. Combined Force Ramp and Equilibrium High-Resolution Investigations Reveal Multipath Heterogeneous Unfolding of Protein G. *J. Phys. Chem. B* **2018**, *122*, 11155−11165.

DOI: 10.1021/acs.jpca.9b08282
J. Phys. Chem. A 2019, 123, 9612−9620